Biophysical Journal
Article

Biophysical Society

Analysis of Baboon IAPP Provides Insight into Amyloidogenicity and Cytotoxicity of Human IAPP

Zachary Ridgway,[1] Kyung-Hoon Lee,[2] Alexander Zhyvoloup,[3] Amy Wong,[1] Charles Eldrid,[3] Eleni Hannaberry,[1] Konstantinos Thalassinos,[3] Andisheh Abedini,[1,*] and Daniel P. Raleigh[1,3,*]
[1]Department of Chemistry, Stony Brook University, Stony Brook, New York; [2]Department of Biology, Chowan University, Murfreesboro, North Carolina; and [3]Institute of Structural and Molecular Biology, University College London, London, United Kingdom

ABSTRACT The polypeptide hormone islet amyloid polypeptide (IAPP) forms islet amyloid in type 2 diabetes, a process which contributes to pancreatic β-cell dysfunction and death. Not all species form islet amyloid, and the ability to do so correlates with the primary sequence. Humans form islet amyloid, but baboon IAPP has not been studied. The baboon peptide differs from human IAPP at three positions containing K1I, H18R, and A25T substitutions. The K1I substitution is a rare example of a replacement in the N-terminal region of amylin. The effect of this mutation on amyloid formation has not been studied, but it reduces the net charge, and amyloid prediction programs suggest that it should increase amyloidogenicity. The A25T replacement involves a nonconservative substitution in a region of IAPP that is believed to be important for aggregation, but the effects of this replacement have not been examined. The H18R point mutant has been previously shown to reduce aggregation in vitro. Baboon amylin forms amyloid on the same timescale as human amylin in vitro and exhibits similar toxicity toward cultured β-cells. The K1I replacement in human amylin slightly reduces toxicity, whereas the A25T substitution accelerates amyloid formation and enhances toxicity. Photochemical cross-linking reveals that the baboon amylin, like human amylin, forms low-order oligomers in the lag phase of amyloid formation. Ion-mobility mass spectrometry reveals broadly similar gas phase collisional cross sections for human and baboon amylin monomers and dimers, with some differences in the arrival time distributions. Preamyloid oligomers formed by baboon amylin, but not baboon amylin fibers, are toxic to cultured β-cells. The toxicity of baboon oligomers and lack of significantly detectable toxicity with exogenously added amyloid fibers is consistent with the hypothesis that preamyloid oligomers are the most toxic species produced during IAPP amyloid formation.

SIGNIFICANCE Islet amyloid polypeptide (IAPP) forms islet amyloid in type 2 diabetes, a process which contributes to pancreatic β-cell dysfunction and death. The factors that control the amyloidogenicity and toxicity of human IAPP are not understood. Comparative studies of human and baboon IAPP reveal that both form broadly similar distributions of preamyloid oligomers and confirm that preamyloid intermediates are significantly more toxic to cultured β-cells than IAPP amyloid fibers. The data reveal a role for the N-terminus in modulating toxicity and shows that substitutions at position 25 can strongly influence the rate of amyloid formation. The results aid our understanding of the sequence determinants of IAPP amyloidogenicity and should prove helpful for the design of nontoxic analogs of human IAPP.

INTRODUCTION

Amyloid formation plays a central role in a number of devastating human diseases, including Alzheimer's disease, systemic amyloidosis, and type 2 diabetes (T2D). Islet amyloid polypeptide (IAPP, also known as amylin) is a 37-residue, neuropancreatic polypeptide hormone, which helps to regulate satiety, control gastric emptying, suppress glucagon release from α-cells, and maintain glucose homeostasis (1,2). In T2D, IAPP aggregates to form islet amyloid in the islets of Langerhans (3,4). The process of islet amyloid formation by human IAPP (hIAPP) contributes to β-cell dysfunction in T2D and to islet transplant failure (3–7). Despite the importance of islet amyloid formation, the features that control the polypeptide's amyloidogenicity and toxicity are not understood.

Submitted October 28, 2019, and accepted for publication December 3, 2019.

*Correspondence: andisheh.abedini@stonybrook.edu or daniel.raleigh@stonybrook.edu

Zachary Ridgway and Kyung-Hoon Lee contributed equally to this work.

Editor: David Eliezer.

https://doi.org/10.1016/j.bpj.2019.12.027

IAPP contains an amidated C-terminus and a disulfide-bridged loop between residues 2 and 7. The sequence of IAPP is strongly conserved, and the hormone is found in all mammals studied. However, not all species form islet amyloid, and the ability to form amyloid in vivo and in vitro correlates with the sequence of the polypeptide and with whether or not a species develops T2D (1,8–10). Notably, mice and rats do not form amyloid in vivo, and the mouse and rat polypeptide is nonamyloidogenic in vitro under standard conditions (11). Comparison of the rat and mouse sequence to the sequence of hIAPP, together with early in vitro experiments, leads to the hypothesis that the ability to form amyloid is controlled by the identity of the 20–29 segment (8,11). hIAPP and rat IAPP (rIAPP) differ at six positions, with five of the substitutions located between residues 23 and 29, including three Pro residues at positions 25, 28, and 29 of rIAPP (Fig. 1). The region lying between residues 20 and 29 of IAPP is important for amyloid formation, but it is clear that the sequence in this region is not the sole factor dictating amyloidogenicity (8,11,12). For example, His-18 in hIAPP is replaced by Arg in rIAPP, and the H18R point mutant has been reported to slow amyloid formation by hIAPP (13–18). Other substitutions outside of the 20–29 segment also influence amyloid formation, but the role of residues located within the N-terminal disulfide-bridged loop is not known (17,19,20).

Deducing the sequence determinants of IAPP amyloidogenicity is important for the development of the next generation of soluble analogs for use as adjuncts to insulin therapy and for the potential development of xenobiotic islet transplantation (21–24). The sequence of baboon IAPP (bIAPP) is known, but its ability to form amyloid has not been examined, nor has its potential toxicity toward β-cells been assessed. The baboon polypeptide contains the H18R substitution found in rIAPP but also includes two other nonconservative replacements relative to the human polypeptide: a K1I and an A25T replacement. The K1I substitution is particularly interesting because it is one of the few reported substitutions at position 1 in IAPP and is one of few replacements of Lys-1 found in primate IAPP sequences (Fig. 1). The effects of these substitutions on amyloid formation have not been examined.

Here, we examine the ability of bIAPP to form amyloid, compare its amyloidogenicity to the human polypeptide, test the role of the individual residue differences between bIAPP and hIAPP, and examine the effects of bIAPP and variants on the viability of INS-1 β-cells. Most, but not all, prior studies are consistent with fibrils being much less toxic than prefibril oligomers; however, studies with 10 residue fragments of hIAPP and variant peptides have indicated that amyloid fibrils may be toxic (25). Thus, we compare the effects of bIAPP fibrils and prefibril oligomers on β-cell viability.

The results provide insight into regions of the polypeptide that are important for controlling amyloidogenicity and toxicity. In particular, the data reveal a role for the N-terminus in modulating toxicity and shows that substitutions at position 25 can strongly influence the rate of amyloid formation. The results are discussed in the context of existing models of IAPP amyloid formation. The work also supports the hypothesis that preamyloid oligomers are the most toxic species produced during IAPP amyloid formation.

	1	10	20	30
Human	KCNTATCAT	QRLANFLVHS	SNNFGAILSS	TNVGSNTY
Rat	KCNTATCAT	QRLANFLVRS	SNNLGPVLPP	TNVGSNTY
Black snub-nosed monkey	KCNTATCAT	QRLANFLVRS	SNNFGSILSS	TNVGSNTY
Bolivian squirrel monkey	KCNTATCSM	HRLADFLGRS	GNNFGAILSP	TNVGSNTY
Chimpanzee	KCNTATCAT	QRLANFLVRS	SNNFGAILSS	TNVGSNTY
Cotton-top tamarin	NTATCSM	HRLADFLGRS	SNNFGAILSP	TNVGS
Crab-eating macaque	KCNTATCAT	QRLANFLVRS	SNNFGTILSS	TNVGSNTY
Garnett's greater bushbaby	KCNTATCAT	QRLANFLVRS	SNNFGAVHSP	TNVGSNTY
Gelada	TCNTATCAT	QRLANFLLRS	SNNFGTILSS	TNVGSNTY
Gorilla	KCNTVTCAT	QRLANFLVRS	SNNFGAILSS	TNVGSNTY
Gray mouse lemur	TCNTATCTI	QRLANFLVRY	SNNFGAVHSP	TNVRSNGY
Green monkey	KCNTATCAT	QRLANFLVRS	SNNFGTILSS	TDVGSNTY
Hamadryas baboon	ICNTATCAT	QRLANFLVRS	SNNFGTILSS	TNVGSNTY
Ma's night monkey	KCNTATCSM	HRLADFLGRS	GNNFGAIISP	TNVGSNTY
Northern white-cheeked gibbon	KCNTATCAT	QRLANFLVRS	SNNFGAILSS	TNVGSNTY
Olive baboon	ICNTATCAT	QRLANFLVRS	SNNFGTILSS	TNVGSNTY
Panamanian white-face capuchin	KCNTATCSM	HRLADFLGRS	GNNFGAILSP	TNVGSNTY
Philippine tarsier	KCNTATCAM	QNLAHFLVRS	SNNFGAILSP	TNVGSNTY
Pig-tailed macaque	KCNTATCAT	QRLANFLVRS	SNNFGTILSS	TNVGSDTY
Rhesus macaque	KCNTATCAT	QRLANFLVRS	SNNFGTILSS	TNVGSNTY
Small-eared galago	KCNTATCAT	QRLANFLVRS	SNNFGAVHSP	TNVGSNTY
Sooty mangabey	KCNTATCAT	QRLANFLVRS	SNNFGTILSS	TNVGSNTY
Sumatran orangutan	KCNTATCAT	QRLANFLVRS	SNNFGAILSS	TNVGSNTY
Sunda flying lemur	KCNTATCAT	QRLANFLIRS	GNNLGAVLSP	TNVGSSTY
Ugandan red colobus	KCNTATCAT	QRLANFLVRS	SNNFGPILSS	TNVGSNTY
Western lowland gorilla	KCNTVTCAT	QRLANFLVRS	SNNFGAILSS	TNVGSNTY

FIGURE 1 Sequence alignment of human, rat, and primate IAPP sequences. Residues that differ from the human sequence are depicted in bold with underline. Only a partial sequence is available for the cotton-top tamarin. All complete sequences contain a disulfide bond between Cys2 and Cys7 and have an amidated C-terminus.

MATERIALS AND METHODS

Computational analysis of amyloidogenicity

The predicted amyloidogenicity of the various sequences was calculated using several web-based amyloid prediction programs: AGGRESCAN, http://bioinf.uab.es/aggrescan/; FoldAmyloid; Zygreggator; and TANGO, http://www.switchlab.org/bioinformatics/tango.

Peptide synthesis and purification

hIAPP, bIAPP, and hIAPP variants were prepared using solid-phase peptide synthesis using standard Fmoc (9-fluorenylemethyloxycarbonyl) methods. Syntheses were conducted on a 0.1-mmol scale, using a CEM Liberty Blue automated microwave peptide synthesizer (CEM, Matthews, NC). CEM ProTide rink amide resin (CEM) was used to obtain the naturally occurring amidated C-terminus. Fmoc-protected pseudoproline (oxazolidine) dipeptide derivatives (Aapptec, Louisville, KY) were used as previously described (26,27). The first amino acid attached to the resin, pseudoproline dipeptide derivatives, arginine, and all β-branched amino acids were double coupled. A trifluoroacetic acid (TFA)-based cocktail (92.5% TFA, 2.5% triisopropylsilane, 2.5% 3,6-Dioxa-1,8-octanedithiol, and 2.5% H_2O) was used to cleave synthesized peptides from the resin and scavenge side-chain-protecting groups. Peptides were oxidized to form a disulfide bond between residues Cys2 and Cys7 in 100% dimethyl sulfoxide with gentle shaking at room temperature for 3 days. Crude peptides were dissolved in 15% acetic acid (v/v) and lyophilized after cleavage. Reverse-phase high performance liquid chromatography (HPLC) was used to purify the crude peptides. Hydrochloric acid was used as an ion-pairing agent instead of TFA because TFA can influence IAPP aggregation kinetics and cell toxicity assays. Residual scavengers were removed by dissolving the dried peptides in 1, 1, 1, 3, 3, 3-Hexafluoro-2-propanol to extract trace amounts of scavengers and were then repurified with reverse-phase HPLC. The purity of the peptides was checked by reverse-phase HPLC using a C18 analytical column (Higgins Analytical, Mountain View, CA). The molecular weights of the purified peptides were confirmed by mass spectrometry via matrix-assisted laser desorption ionization time-of-flight mass spectrometry: IAPP expected, 3902.8; IAPP observed, 3903.3; bIAPP expected, 3936.9; bIAPP observed, 3937.4; K1I-IAPP expected, 3887.9; K1I-IAPP observed, 3888.3; H18R-IAPP expected 3922.4; H18R-IAPP observed, 3921.5; A25T-IAPP expected, 3932.9; A25T-IAPP observed, 3933.3.

Sample preparation

Dry peptides were dissolved in 100% 1, 1, 1, 3, 3, 3-Hexafluoro-2-propanol at room temperature for 4 h at a target concentration of 0.8 mM. Aliquots were filtered through a 0.22-μm Millex syringe-driven filter (GE Healthcare, Chicago IL). 10 μL aliquots of stocks were lyophilized overnight and reconstituted in phosphate-buffered saline (PBS) to determine concentration. The concentration was determined by measuring the absorbance at 280 nm. After concentration determination, aliquots were lyophilized for various experiments.

Thioflavin-T fluorescence assays

Thioflavin-T-binding assays were employed to monitor amyloid formation as a function of time using a Molecular Devices SpectraMax Gemini EM microplate reader (Molecular Devices, San Jose, CA) and were measured using 450 nm of excitation and 485 nm of emission. Corning 96-well nonbinding surface black plates with lids (VWR International) were used for all assays, and plates were sealed with polyethylene-sealing tape. Lyophilized peptide aliquots were dissolved in a buffer and thioflavin-T solution immediately before measurements. All the experiments used 16 μM IAPP, 32 μM thioflavin-T in PBS (pH 7.4) at 25°C, with no agitation.

Photochemical cross-linking

Samples were cross-linked using Tris (bipyridyl) Ru(II) chloride ($Ru(bpy)_3$) in the presence of ammonium persulfate (APS). The molar ratios of $Ru(bpy)_3$, APS, and peptide were 3.5:70:1, respectively. Samples were dissolved in a buffer (PBS (pH 7.4)) and were centrifuged for 10 min at 15,000 $\times$ g before the reaction. In a typical reaction, 2.5 μL of $Ru(bpy)_3$ and APS were added to a 15 μL aliquot of 40 μM peptide and irradiated for 10 s with a 140-W incandescent bulb. After the reaction, solutions were quenched with 10 μL of tricine sample buffer containing 5% β-mercaptoethanol. Samples were then heated for 5 min at 85°C before loading on the gel. Gels were visualized by silver staining, and gel densitometry was performed using GelAnalyzer version 2010a. The relative intensity of each band was calculated by first correcting the baseline, then integrating the area under each peak.

TEM

Transmission electron microscopy (TEM) images were captured with an FEI Bio TwinG^2 transmission electron microscope (FEI, Hillsboro, OR). Samples were blotted on a carbon-coated formvar 300-mesh copper grid for 1 min and then negatively stained with 2% uranyl acetate for 1 min.

Cytotoxicity assays

INS-1 cells were purchased from AddexBio and cultured with optimized RPMI-1640 (#C0004-02; AddexBio, San Diego, CA) medium supplemented with 10% ultralow IgG FBS (#16250078; Gibco, Gaithersburg, MD). CellTiter-Glo 2.0 (#G9242; Promega, Madison, WI) assays were used to evaluate the cytotoxicity of hIAPP, bIAPP, and hIAPP variants toward INS-1 β-cells. Cells were seeded at ~50% confluence on a 96-well half-area clear bottom white plates (#675083; Greiner, Kremsmünster, Austria) and incubated for 36 h in a 5% CO_2 humidified incubator at 37°C. Serial dilutions of the peptides were freshly prepared before use from lyophilized peptide. Cells were exposed to varying concentrations of peptide diluted in fresh complete medium for 24 h. For CellTiter-Glo 2.0 assays, the culture plates were cooled to room temperature, and an equal volume of the assay reagent was added to the treated cells. Plates were vigorously (700 rpm) shaken for 1 min, and the luminescence intensity was measured using a Clariostar plate reader (BMG Labtech, Cary, NC). Statistical analysis and calculation of EC_{50}-values were conducted using Graph Pad Prism 5. INS-1 cells and Chinese hamster ovary (CHO)-T cells were used to independently compare the toxicity of hIAPP and bIAPP amyloid fibers and prefibrillar species. CHO-T cells were kindly provided by Professor Ivan Gout.

Ion-mobility mass spectrometry

Lyophilized samples were dissolved in 100% liquid chromatography-mass spectrometry-grade dimethyl sulfoxide to a concentration of 3.2 mM and incubated at 37°C for 24 h to ensure the breakup of any preformed fibrils or other aggregates before analysis. After incubation, samples were diluted 100-fold using 100 mM ammonium acetate solution (pH 7.4) to a working concentration of 32 μM peptide and immediately infused into a Synapt G1 (Waters, Wilsmslow, UK) mass spectrometer, using capillaries produced in house (borosilicate glass capillaries extruded using a Flaming Brown P97 micropipette puller (Sutter Instrument, Novato, CA) and then coated in gold using a Quorum 150QR S sputter coater (Laughton, UK)).

Mass calibration was conducted using cesium iodide clusters formed from a 30 mg/mL solution of cesium iodide in water. Collision cross section (CCS) calibration was performed using a mixture of polyethylene oxide (PEO) (5 μM PEO, 10 μM NaCl in liquid chromatography-mass spectrometry-grade methanol) and peptides from equine cytochrome C digested by trypsin (0.5 mg/mL in 49:49:2 (v/v) % of water/methanol/acetic acid

solution) (28–30). CCS calculations were performed as described by Thalassinos et al. (31). Data were collected using the following parameters: capillary 1.4 kV, sampling cone of 40 V, extraction cone of 1.0 V, backing pressure of 4.50 mbar, trap CE of 15 eV, transfer CE of 13 eV, bias of 16 V, IMS wave velocity of 250 ms^{-1}, IMS wave height of 6.0 V.

RESULTS

The primary sequences of bIAPP and hIAPP are shown in Fig. 1 and compared to other primate IAPP sequences. The rat IAP sequence is also included for comparison. The three substitutions in bIAPP relative to hIAPP are predicted to have different effects on amyloidogenicity, and it is not known whether bIAPP has a different propensity to form amyloid than hIAPP (Table S1). Lys-1 in IAPP is strongly conserved in IAPP, and the Lys-1-to-Ile replacement is one of only a very few known substitutions at this position. In fact, very few substitutions are found within the first seven residues of IAPP, and the K1I replacement is an example of a rare substitution, relative to hIAPP, that changes the charge in this region. The K1I substitution reduces the net charge on IAPP at all relevant pH values and hence could influence solubility and amyloidogenicity. hIAPP has a net charge of between 2 and 4 at physiological pH depending upon the exact pKa-values of the N-terminus and His-18 side chain, whereas bIAPP will have a net charge between 1 and 3.

The locations of the substitutions found in bIAPP are in unique environments in the hIAPP amyloid fibril structure. The Eisenberg model of the hIAPP fibril, derived from x-ray crystal structure studies of IAPP fragments, indicates that the fibril layer is made up of two columns of IAPP monomers, with each monomer adopting a U-shaped structure (32). There are two symmetrically related monomers per layer of the fibril (Fig. 2 *B*). Each monomer in a fibril layer contributes an N-terminal and C-terminal β-strand to the ordered part of the fibril. His18 lies at the end of the N-terminal strand, and Ala25 is at the beginning of the C-terminal strand, with a disordered region between these two residues. Lys1, along with the disulfide loop, is excluded from the amyloid core in this model and in the solid-state NMR model (33). Although the 1–7 region does not participate in the amyloid core, previous work has shown the presence of the disulfide influences amyloid formation (34). His18 points inward in the fibril layer (Fig. 2 *C*), in proximity to Ile26 and Asn22. Replacement of His18 with Arg, as found in bIAPP, may lead to steric effects during fibril formation and to changes in desolvation energetics. The Ala25 side chain projects outwards toward the opposing monomer in the same layer in proximity to Asn35. The 23–27 region has been hypothesized to form a transient β-sheet intermediate along the misfolding pathway of hIAPP (12). Substituting Ala 25 to Thr would increase the propensity of this region to form β-sheets because Thr has a significantly higher β-sheet propensity than Ala.

Standard amyloid prediction algorithms predict that the Ile substitution at position 1 will either enhance amyloidogenicity or will have no effect (35–39). AGGRESCAN, FoldAmyloid, and Zygreggator all predict an enhancement in amyloidogenicity, whereas TANGO predicts that the replacement will have very little effect. The replacement of His18 in hIAPP with an Arg is a common substitution (Fig. 1). Arg is found at position 18 in monkey and macaque IAPP, both of which are amyloidogenic, but is also found in the nonamyloidogenic rIAPP (Fig. 1). Substitution of His-18 with Arg in hIAPP has been reported to reduce its amyloidogenicity, as does reducing the pH to ensure that His18 is fully charged (13–16,18). The AGGRESCAN, TANGO, and Zygreggator programs predict that the His to Arg replacement reduces amyloidogenicity, whereas FoldAmyloid predicts only a modest impact.

The final substitution in bIAPP relative to hIAPP is the replacement of Ala25 in hIAPP with Thr in bIAPP. Position 25 lies in the region initially proposed to be the critical amyloidogenic determinant of IAPP (11). More recent work indicates that hIAPP formation in vitro may involve the

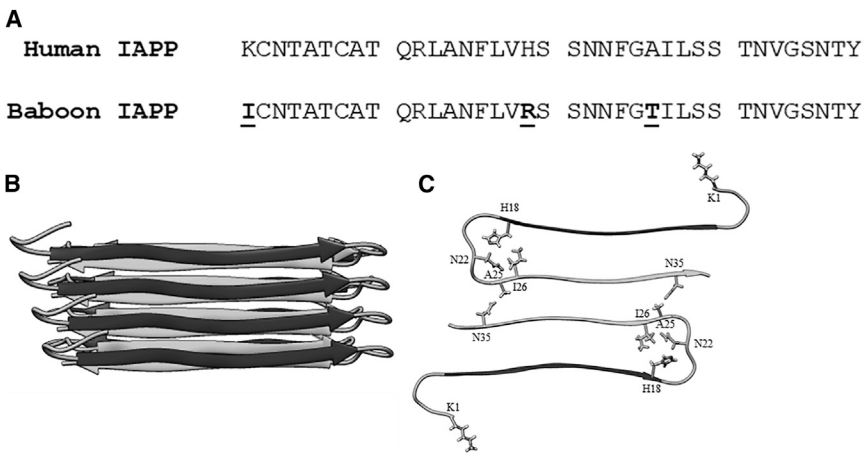

FIGURE 2 Comparison of the sequence of hIAPP and bIAPP and location of substitutions within a fibril model. (*A*) A comparison of hIAPP and bIAPP primary sequences is shown here. Both polypeptides contain a disulfide bond between residues Cys2 and Cys7 and have an amidated C-terminus. Residues in bIAPP that differ from hIAPP are depicted in bold with underline. (*B*) A side view of the IAPP fibril model is shown here. (*C*) A top-down view of one layer in the fibril structure, with sites of mutation and neighboring residues shown in stick format, is given.

formation of an obligatory intermolecular β-sheet in this region, which is then disrupted as the polypeptides rearrange to form the final amyloid fibril structure (12). Thr is a relatively nonconservative mutation for Ala. The change significantly decreases α-helical propensity, increases β-sheet propensity, and introduces hydrogen bonding functionality into the side chain. The AGGRESCAN, Zygreggator, and TANGO programs all predict that this substitution reduces amyloidogenicity, whereas FoldAmyloid predicts no significant effect. The complete bIAPP sequence is predicted to be less amyloidogenic by TANGO and Zyggregator, whereas AGGRESCAN predicts that bIAPP is more amyloidogenic than hIAPP, and FoldAmyloid predicts that both peptides have similar core amyloidogenic regions (Table S1).

bIAPP forms amyloid on the same timescale as hIAPP

We first examined amyloid formation by bIAPP and compared it to hIAPP using fluorescence-detected thioflavin-T-binding assays together with TEM. Thioflavin-T is a small dye whose quantum yield increases upon binding to amyloid fibrils (40–42). The dye is an extrinsic probe, but it has been shown to report accurately on the kinetics of hIAPP amyloid formation under the conditions used here. However, there are cases in which fluorescence of the dye does not noticeably increase in the presence of amyloid (43). In addition, the relationship between the intensity of thioflavin-T fluorescence and the amount of amyloid formed is not clear. Thus, we used TEM to confirm the results of the thioflavin-T assays.

Amyloid formation by hIAPP is composed of three phases: an initial lag phase that does not generate any significant thioflavin-T response, followed by a growth phase in which amyloid fibrils elongate and a final plateau stage in which fibrils are in equilibrium with soluble peptide. This sequence of events gives rise to a sigmoidal plot of thioflavin-T fluorescence versus time. We studied amyloid formation in PBS (10 mM phosphate, 140 mM KCl). As shown in Fig. 3 *A*, both the human and baboon peptides exhibit sigmoidal thioflavin-T fluorescence curves, as expected for an amyloidogenic IAPP. T_{50}, the time required to achieve 50% of the total fluorescence gain in a thioflavin-T assay, is 4.6 $\pm$ 0.3 h for hIAPP in PBS. A separate batch of hIAPP was independently analyzed and yielded a T_{50} of 3.3 $\pm$ 1.0 h. We report the average of these two measurements, 4.0 $\pm$ 1.0 h, in Table 1. The baboon polypeptide forms amyloid at a similar rate to hIAPP in PBS with a T_{50} of 2.9 $\pm$ 0.4. Aliquots were removed from each kinetic experiment after 24 h, a time sufficient for both peptides to reach the thioflavin-T fluorescence plateau, and TEM images were recorded (Fig. 3, *B* and *C*). Clear mats of amyloid fibrils were observed in the images of both peptides.

bIAPP populates low-order oligomers during the lag phase of amyloid formation

Amyloid formation by hIAPP is believed to proceed through the formation of low-order oligomers (44–47). We conducted comparative photochemical cross-linking studies to test whether this is also the case for bIAPP. Peptides were dissolved in solution, and the photoinduced cross-linking of unmodified proteins (PICUP) in situ method of Teplow and co-workers was used to probe the distribution of oligomers (48). A distribution of oligomeric species ranging from monomers to hexamers is observed for the baboon polypeptide during the lag phase, with noticeably higher populations of monomer, dimer, and trimer than of higher-order species (Fig. 4 *A*). Previously reported control experiments with hIAPP show that these distributions fundamentally differ from one expected for a monomeric peptide of similar size that forms cross-links by random collisions in the solution (49). Quantitative analysis of the silver-stained gels reveals

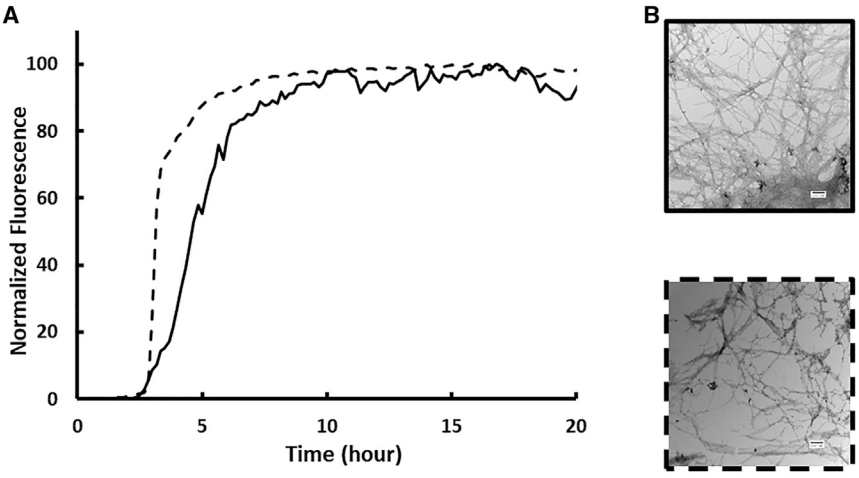

FIGURE 3 bIAPP forms amyloid on the same timescale as hIAPP in PBS. (*A*) Thioflavin-T fluorescence assays of amyloid formation by hIAPP (*solid*) and bIAPP (*dashed*) are shown here. (*B*) TEM images of amyloid fibrils formed by hIAPP (*solid*) and bIAPP (*dashed*) are shown here. Experiments were conducted at 25°C (pH 7.4) PBS with 16 μM IAPP. Scale bars represent 100 nm.

TABLE 1 T_{50}-Values of hIAPP, bIAPP, and Point Mutants of bIAPP

Peptide	T_{50} (h)
hIAPP	4.0 ± 1.0
bIAPP	2.9 ± 0.4
K1I-IAPP	5.8 ± 0.8
H18R-IAPP	11.4 ± 0.2
A25T-IAPP	0.8 ± 0.1

Uncertainties represent apparent standard deviations.

that the distribution of oligomers populated by bIAPP and hIAPP are broadly similar. Although there are some differences in the relative intensities, the relative population of pentamers and hexamers is higher for hIAPP compared to bIAPP, whereas the relative population of lower-order oligomers is higher for bIAPP (Fig. 4 *B*). However, we are hesitant to draw any firm quantitative conclusions from these differences because they could arise from genuine differences in oligomeric distributions, from intrinsic differences in cross-linking efficiency, or both. PICUP targets multiple amino acids but particularly Trp, Tyr, Met, Cys, and (to a lesser extent) Phe and His. The difference in primary sequence (particularly the H18R mutation) may thus contribute to the observed differences (48). The key point is both polypeptides form low-order oligomers during the lag phase with distributions that differ from that expected for a monomeric polypeptide, which forms cross-links by random collisions.

IM-MS analysis shows hIAPP and bIAPP have similar collisional cross sections but different arrival time distributions

Within 5 min of dilution, monomeric and dimeric species were detected for both hIAPP and bIAPP (Fig. 5, *A* and *B*), with the main species in the spectrum corresponding to the +3 monomer (1^{+3}). hIAPP and bIAPP display different arrival-time distributions (ATDs) while having similar overall collision cross sections (CCSs) (Fig. 5, *C* and *D*). For the monomeric species, the 1^{+2} and 1^{+3} ions display similar ATDs and CCSs. The 1^{+2} species of both polypeptides have broad ATD peaks, suggesting a dynamic conformation. Both the human and baboon 1^{+4} states display two distinct conformations, a compact and extended state, and the most noticeable difference is that the human polypeptide populates the extended state much less. For the dimeric species, the 2^{+4} baboon and human polypeptide have very similar CCS-values; however, the bIAPP ion displays a long tail of compact conformations. The 2^{+5} charge state is the only species in which hIAPP and bIAPP differ noticeably in CCS-value, in which the baboon polypeptide has a higher CCS and wider ATD, suggesting a more extended and dynamic conformation than hIAPP. Collectively, these results suggest that bIAPP monomers and dimers are both more dynamic and populate more open conformations than hIAPP.

Mutational analysis of amyloid formation by hIAPP

We next examined the effect of individually substituting the baboon residues into hIAPP. The results of the H18R substitution have been reported to lead to a reduction in amyloidogenicity at pH 7.4, but the effects of the substitutions at Lys-1 and at Ala-25 have not been studied (14,18). We synthesized the peptides and tested their ability to form amyloid in PBS (Fig. 6 *A*). We first examined the effect of the H18R replacement under the conditions of our assays. Consistent with previous results, the mutation leads to an increase in the value of T_{50}, which is 11.4 ± 0.2 h under the conditions used in this work. K1I-IAPP forms amyloid at a slightly slower rate than hIAPP, even though several amyloid prediction programs predict that the mutant should be more amyloidogenic than hIAPP. The T_{50} for K1I-IAPP was found to be 5.8 ± 0.8 h in PBS compared to 4.0 ± 1.0 h for hIAPP. The difference is unlikely to be significant. The A25T-IAPP variant was found to form amyloid noticeably faster than the other polypeptides, although amyloid prediction programs all predicted that this mutant should be less amyloidogenic than hIAPP. The T_{50} for A25T-IAPP was 0.8 ± 0.1 h in PBS. TEM imaging confirms the presence of fibrils in samples from all variants (Fig. 6 *B*).

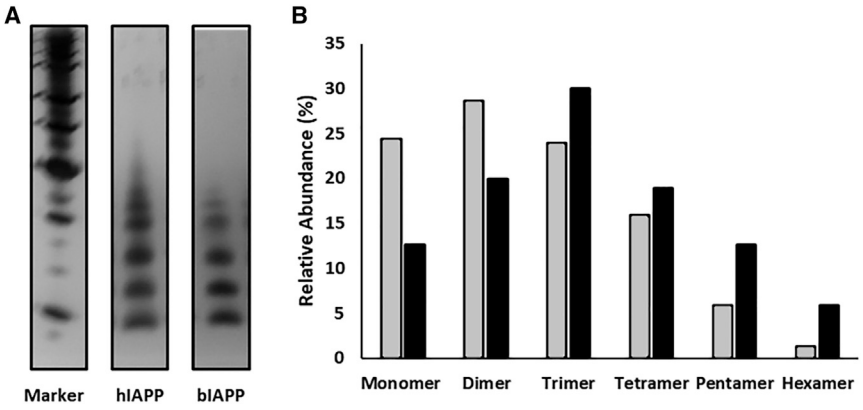

FIGURE 4 Human and baboon IAPP form oligomers. (*A*) Silver-stained SDS-PAGE gel showing the distribution of oligomer species populated by hIAPP and bIAPP at 40 μM is given. (*B*) Relative abundance of IAPP in oligomeric species detected via PICUP experiments with hIAPP (*black*) and bIAPP (*gray*) is shown. Relative abundances were derived from the silver-stained gel in (*A*).

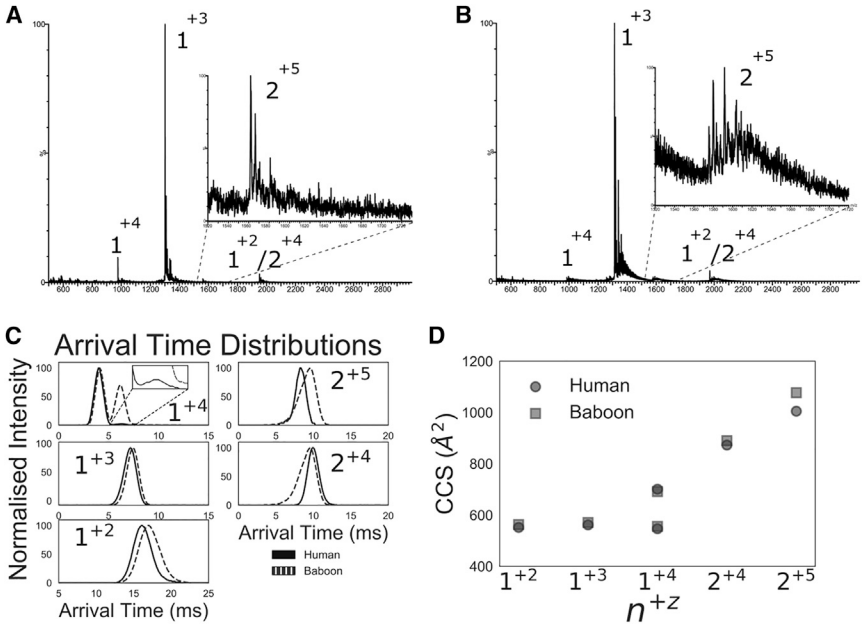

FIGURE 5 IM-MS of hIAPP and bIAPP. (*A*) Shown here is the mass spectrum of hIAPP, inset: lowly populated +5 dimeric charge state. (*B*) Shown here is the mass spectrum of bIAPP, inset: lowly populated +5 dimeric charge state. (*C*) Shown here are the overlaid ATDs for hIAPP (*solid*) and bIAPP (*dashed*), and the inset shows lowly populated extended conformation for hIAPP 1^{+4}.(*D*) CCS-values for hIAPP (*black*) and bIAPP (*gray*) are shown. Notation of charge states is n^{+z}, where n is the oligomeric state and z is the charge state.

We also conducted photochemical cross-linking studies of the three-point substitutions (Fig. S1). All point variants studied showed a distribution of oligomers similar to hIAPP. Monomer through hexamer species are detected, with relative abundances of protein in n-mer species being nearly identical to hIAPP and differing from those observed for bIAPP. This suggests that no individual substitution is responsible for the apparent differences in the distribution of oligomers observed for bIAPP relative to hIAPP.

bIAPP is toxic to cultured β-cells, and amyloid fibers are less toxic than preamyloid oligomers

Having established that bIAPP forms amyloid, we next examined its effect on the viability of cultured β-cells using the rat INS-1 β-cell line. Dose-response experiments were conducted by measuring global cellular ATP levels (CellTiter-Glo) (Fig. 7). Exposure of β-cells to bIAPP induces a reduction in cell viability in a dose-dependent manner. The effective concentration needed to generate half the maximal response, $EC_{50,}$ was similar for hIAPP and bIAPP: 43 μM for bIAPP and 40 μM for hIAPP.

We next examined the effect of the three substitutions (K1I, H18R, and A25T) on the toxicity of hIAPP. The H18R variant behaved similarly to wild-type hIAPP, with an EC_{50}-value of 41.9 μM. However, we repeated the experiment with independently prepared batches of H18R-IAPP and hIAPP and found that the ratio of the EC_{50}-values differed by a factor of two in this case, with H18R-IAPP being less toxic. We also repeated the thioflavin-T kinetic experiments and observed T_{50}-values of 3.3 $\pm$ 1.0 h for the wild-type and 10.1 $\pm$ 2.6 h for the H18R variant. These values are statistically similar to the results summarized in Table 1. The difference in EC_{50}-values arises because of a small variation in the EC_{50} of the second batch of H18R-IAPP (46.8 μM) and in the EC_{50} of the second batch of wild-type IAPP (23 μM). The toxicity of H18R-IAPP has been found to be reduced relative to hIAPP in other studies

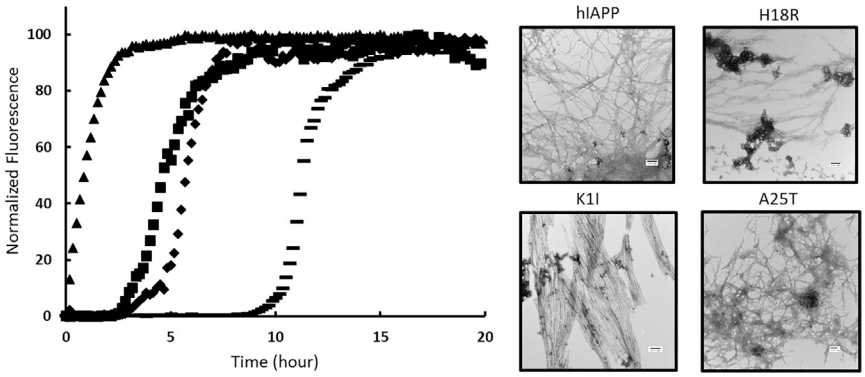

FIGURE 6 Mutational analysis of amyloid formation by human IAPP. (*A*) Thioflavin-T fluorescence assays of amyloid formation by human IAPP (*square*), K1I human IAPP (*diamond*), A25T human IAPP (*triangle*), and H18R human IAPP (*bar*) are shown here. (*C*) A TEM image of fibrils formed by human IAPP, K1I-IAPP, A25T-IAPP, and H18R-IAPP is shown here. Experiments were conducted at 25°C (pH 7.4) PBS with 16 μM IAPP. Scale bars represent 100 nm.

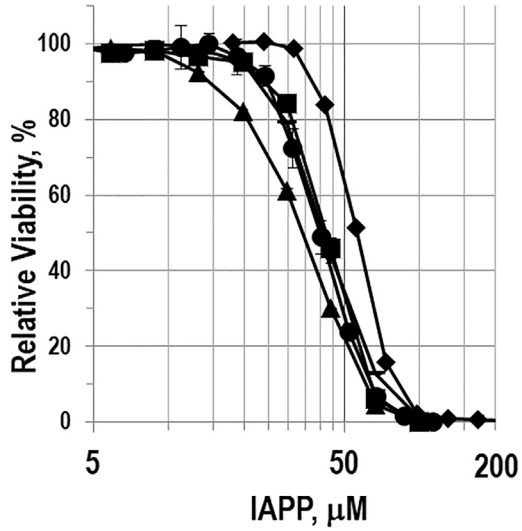

FIGURE 7 Viability of cultured INS-1 β-cells after exposure to hIAPP (*square*), bIAPP (*circle*), K1I-IAPP (*diamond*), H18R-IAPP (*bar*), and A25T-IAPP (*triangle*) as measured using the CellTiter-Glo assay. The *x* axis is plotted with a logarithmic scale.

(18). The reasons for the slightly different results reported here relative to prior studies are not clear. They may reflect the use of different cell lines, different assays of cell viability, differences in minor impurities, differences in the counterion present in the preparation of IAPP variants (TFA is the most common counterion in IAPP preparations; the peptides studied here were prepared with chloride as the counterion), or a combination of these factors. The A25T-IAPP variant had a slightly different dose-response curve then human IAPP and bIAPP, with an EC_{50}-value of 34.1 μM. K1I-IAPP elicited the lowest toxic response, with an EC_{50} of 55.6 μM (Table 2). These differences are modest, and we are hesitant to ascribe strong significance, although they are statistically different. We next compared the effect of preformed amyloid fibrils on cell viability. Neither hIAPP or bIAPP amyloid fibrils were significantly toxic toward INS-1 β-cells or CHO-T cells (Fig. S2).

DISCUSSION

The data presented here show that bIAPP is similar to IAPP derived from other primates in the sense that it forms amyloid and does so on the same timescale as hIAPP. Both polypeptides form low-order oligomers in the lag phase of amyloid formation with broadly similar distributions, though differences are seen. Both bIAPP and hIAPP are toxic to cultured pancreatic β-cells, with preamyloid oligomers being much more toxic than mature fibers. The similar toxicity of hIAPP and bIAPP and their similar rates of amyloid formation indicate that the differences in properties detected by ion-mobility mass spectrometry (IM-MS) and by photochemical cross-linking do not correlate with toxicity or amyloidogenicity in this case. We believe the key point is that both polypeptides form low-order oligomer species and that prefibril species are the most toxic. Overall, the data is consistent with the hypothesis that soluble preamyloid oligomers are the most toxic species produced during IAPP amyloid formation.

TABLE 2 EC_{50} Values of hIAPP, bIAPP, and Variants of bIAPP

Peptide	EC_{50} (μm)	SEM
bIAPP	43.0	1.2
hIAPP[a]	40.0	1.9
K1I-IAPP	55.6	0.7
H18R-IAPP[a]	41.9	0.9
A25T-IAPP	34.1	1.6

Uncertainties represent SEM.

[a]These experiments were repeated with different batches of hIAPP and H18R-IAPP. In this case, the EC_{50} of the human peptide was measured to be 22.8 $\pm$ 0.7 μm, and the value for H18R-IAPP was measured to be 46.8 $\pm$ 1.0 μm.

Cell toxicity assays revealed that substitutions found in bIAPP have relatively small effects on cell viability. The data indicate that the K1I replacement as position 1 has a moderate, but detectable, effect on toxicity. This indicates that the identity of the residues in the N-terminal region of hIAPP make contributions to the toxicity of IAPP. This region may thus offer additional sites to target during efforts to redesign hIAPP to produce more soluble, less aggregation-prone variants.

The analysis of the point variants K1I and A25T provides insight into the factors that help control IAPP's ability to form amyloid. The K1I replacement in hIAPP is a rare example of a replacement at position 1 and also a rare example of a sequence change in the first 16 residues of IAPP that alters the net charge (Fig. 1). Previous studies have reported that removal of the first seven residues of hIAPP had modest effects on the T_{50} for amyloid formation (50).

It is interesting to note that the K1I mutation has only modest effects on amyloid formation in PBS even though the net charge of the polypeptide is reduced. The timescale of IAPP amyloid formation depends on the choice of buffer, ionic strength, and anionic species present (51,52). We have found that hIAPP amyloid formation is faster in the phosphate buffer than in the Tris buffer and have even observed that the relative rates of amyloid formation between hIAPP and some variants can be reversed between Tris and PBS. This is believed to reflect the fact that phosphate interacts more strongly with IAPP than does Tris. These observations help rationalize the apparent surprising result that the K1I mutation has little effect on the timescale of amyloid formation in PBS. Removal of the positive charge is expected to accelerate the rate of amyloid production, but removal of the charge is also expected to reduce interactions with phosphate, and this effect will slow amyloid formation. The net result is an overall modest effect. A similar behavior has been observed with a 2–37 fragment of hIAPP that lacks Lys-1 (53).

The results with the A25T substitution highlight the importance of this region of the polypeptide and also highlight the difficulties with current methods to predict amyloidogenicity. The mutant forms amyloid faster than the wild-type, even though it is predicted to be less amyloidogenic. The molecular basis for the more-rapid aggregation is not understood, but the replacement may alter the stability of the transient β-sheet intermediate that has been recently identified by time-resolved 2D-IR (12). Replacement of Ala with Thr leads to an increased β-sheet propensity and a decreased α-helical propensity and also introduces a hydrogen-bonding functionality into the side chain, which could contribute to stabilizing intermolecular side chain-side chain interactions. Along these lines, it is interesting to examine cross-strand pairing propensities in parallel β-sheets. Statistical analysis of pairing preferences between adjacent strands in parallel β-sheets in globular proteins indicates that Thr-Thr pairs occur more frequently than expected based on the relative abundance of Thr in parallel β-sheets, whereas Ala-Ala pairs occur less frequently than expected based on the relative abundance of Ala in parallel β-sheets (54,55). The differences in cross-strand pairing frequencies reflect the packing across the strands; an Ala-Ala pair is considerably smaller than a Thr-Thr pair and may introduce an instability in the β-sheet by creating a gap and thus be less favored than the Thr-Thr pair. In addition, an array of in-register Thr residues can form a hydrogen-bonded "ladder" that will stabilize a parallel β-sheet. Such interactions have been observed in at least one structure of fibrils from by a prion (56).

SUPPORTING MATERIAL

Supporting Material can be found online at https://doi.org/10.1016/j.bpj.2019.12.027.

AUTHOR CONTRIBUTIONS

Z.R. conducted and designed experiments, analyzed data, and wrote the manuscript. K.-H.L. conducted experiments, analyzed data, and prepared critical reagents. A.Z. conducted experiments, designed protocols, and analyzed data. A.W. conducted experiments and analyzed data. E.H. conducted experiments. C.E. conducted experiments, analyzed data, and assisted with manuscript preparation. K.T. designed experiments, analyzed data, and helped supervise research. A.A. designed and conducted experiments, analyzed data, helped design the project, and assisted with manuscript preparation. D.P.R. designed project, directed and supervised research, and wrote the manuscript.

ACKNOWLEDGMENTS

We thank members of the Raleigh and Thalassinos groups for helpful discussions and Ms. Daeun Noh for supplying the sequence alignment of primate IAPP sequences. We thank Prof. David Eisenberg for providing the coordinates of the hIAPP amyloid fibril model.

This work was supported by grants from the United States National Institutes of Health, GM078114, and American Heart Association award 17SDG33410350. A.Z. was supported by Wellcome Trust award 107927/Z/15/Z. Z.R. was supported in part by a National Institute of Health training grant 5T32GM09271405. C.E. was supported by Biotechnology and Biological Sciences Research Council iCASE PhD studentship with Waters BB/L015382/1. The IM-MS spectrometry was purchased via Wellcome Trust Multiuser equipment grant 104913/Z/14/Z to K.T.

REFERENCES

1. Westermark, P., A. Andersson, and G. T. Westermark. 2011. Islet amyloid polypeptide, islet amyloid, and diabetes mellitus. *Physiol. Rev.* 91:795–826.
2. Lutz, T. A. 2010. The role of amylin in the control of energy homeostasis. *Am. J. Physiol. Regul. Integr. Comp. Physiol.* 298:R1475–R1484.
3. Westermark, P., C. Wernstedt, …, K. H. Johnson. 1987. Amyloid fibrils in human insulinoma and islets of Langerhans of the diabetic cat are derived from a neuropeptide-like protein also present in normal islet cells. *Proc. Natl. Acad. Sci. USA.* 84:3881–3885.
4. Abedini, A., and A. M. Schmidt. 2013. Mechanisms of islet amyloidosis toxicity in type 2 diabetes. *FEBS Lett.* 587:1119–1127.
5. Cooper, G. J., A. C. Willis, …, K. B. Reid. 1987. Purification and characterization of a peptide from amyloid-rich pancreases of type 2 diabetic patients. *Proc. Natl. Acad. Sci. USA.* 84:8628–8632.
6. Westermark, G. T., P. Westermark, …, O. Korsgren; Nordic Network for Clinical Islet Transplantation. 2008. Widespread amyloid deposition in transplanted human pancreatic islets. *N. Engl. J. Med.* 359:977–979.
7. Potter, K. J., A. Abedini, …, C. B. Verchere. 2010. Islet amyloid deposition limits the viability of human islet grafts but not porcine islet grafts. *Proc. Natl. Acad. Sci. USA.* 107:4305–4310.
8. Betsholtz, C., L. Christmansson, …, P. Westermark. 1989. Sequence divergence in a specific region of islet amyloid polypeptide (IAPP) explains differences in islet amyloid formation between species. *FEBS Lett.* 251:261–264.
9. Akter, R., R. L. Bower, …, D. P. Raleigh. 2018. Amyloidogenicity, cytotoxicity, and receptor activity of bovine amylin: implications for xenobiotic transplantation and the design of nontoxic amylin variants. *ACS Chem. Biol.* 13:2747–2757.
10. Akter, R., A. Abedini, …, D. P. Raleigh. 2017. Evolutionary adaptation and amyloid formation: does the reduced amyloidogenicity and cytotoxicity of ursine amylin contribute to the metabolic adaption of bears and polar bears? *Isr. J. Chem.* 57:750–761.
11. Westermark, P., U. Engström, …, C. Betsholtz. 1990. Islet amyloid polypeptide: pinpointing amino acid residues linked to amyloid fibril formation. *Proc. Natl. Acad. Sci. USA.* 87:5036–5040.
12. Buchanan, L. E., E. B. Dunkelberger, …, M. T. Zanni. 2013. Mechanism of IAPP amyloid fibril formation involves an intermediate with a transient β-sheet. *Proc. Natl. Acad. Sci. USA.* 110:19285–19290.
13. Green, J., C. Goldsbury, …, U. Aebi. 2003. Full-length rat amylin forms fibrils following substitution of single residues from human amylin. *J. Mol. Biol.* 326:1147–1156.
14. Jha, S., J. M. Snell, …, A. T. Alexandrescu. 2014. pH dependence of amylin fibrillization. *Biochemistry.* 53:300–310.
15. Chargé, S. B., E. J. de Koning, and A. Clark. 1995. Effect of pH and insulin on fibrillogenesis of islet amyloid polypeptide in vitro. *Biochemistry.* 34:14588–14593.
16. Abedini, A., and D. P. Raleigh. 2005. The role of His-18 in amyloid formation by human islet amyloid polypeptide. *Biochemistry.* 44:16284–16291.
17. Knight, J. D., J. A. Hebda, and A. D. Miranker. 2006. Conserved and cooperative assembly of membrane-bound alpha-helical states of islet amyloid polypeptide. *Biochemistry.* 45:9496–9508.
18. Khemtemourian, L., G. Guillemain, …, J. A. Killian. 2017. Residue specific effects of human islet polypeptide amyloid on self-assembly and on cell toxicity. *Biochimie.* 142:22–30.

19. Abedini, A., and D. P. Raleigh. 2006. Destabilization of human IAPP amyloid fibrils by proline mutations outside of the putative amyloidogenic domain: is there a critical amyloidogenic domain in human IAPP? *J. Mol. Biol.* 355:274–281.
20. Koo, B. W., J. A. Hebda, and A. D. Miranker. 2008. Amide inequivalence in the fibrillar assembly of islet amyloid polypeptide. *Protein Eng. Des. Sel.* 21:147–154.
21. Ratner, R. E., R. Dickey, …, O. G. Kolterman. 2004. Amylin replacement with pramlintide as an adjunct to insulin therapy improves long-term glycaemic and weight control in Type 1 diabetes mellitus: a 1-year, randomized controlled trial. *Diabet. Med.* 21:1204–1212.
22. Kruger, D. F., and M. A. Gloster. 2004. Pramlintide for the treatment of insulin-requiring diabetes mellitus: rationale and review of clinical data. *Drugs.* 64:1419–1432.
23. Wang, H., A. Abedini, …, D. P. Raleigh. 2014. Rationally designed, nontoxic, nonamyloidogenic analogues of human islet amyloid polypeptide with improved solubility. *Biochemistry.* 53:5876–5884.
24. Nguyen, T. M., J. R. Wright, Jr., …, J. M. Conlon. 1995. Characterization of the pancreatic hormones from the Brockmann body of the tilapia: implications for islet xenograft studies. *Comp. Biochem. Physiol. C Pharmacol. Toxicol. Endocrinol.* 111:33–44.
25. Krotee, P., J. A. Rodriguez, …, D. S. Eisenberg. 2017. Atomic structures of fibrillar segments of hIAPP suggest tightly mated β-sheets are important for cytotoxicity. *eLife.* 6:e19273.
26. Marek, P., A. M. Woys, …, D. P. Raleigh. 2010. Efficient microwave-assisted synthesis of human islet amyloid polypeptide designed to facilitate the specific incorporation of labeled amino acids. *Org. Lett.* 12:4848–4851.
27. Abedini, A., G. Singh, and D. P. Raleigh. 2006. Recovery and purification of highly aggregation-prone disulfide-containing peptides: application to islet amyloid polypeptide. *Anal. Biochem.* 351:181–186.
28. Haler, J. R. N., C. Kune, …, E. De Pauw. 2017. Comprehensive ion mobility calibration: poly(ethylene oxide) polymer calibrants and general strategies. *Anal. Chem.* 89:12076–12086.
29. Haler, J. R. N., P. Massonnet, …, E. De Pauw. 2018. Comparison of different ion mobility setups using poly (ethylene oxide) PEO polymers: drift tube, TIMS, and T-wave. *J. Am. Soc. Mass Spectrom.* 29:114–120.
30. Valentine, S. J., A. E. Counterman, and D. E. Clemmer. 1999. A database of 660 peptide ion cross sections: use of intrinsic size parameters for bona fide predictions of cross sections. *J. Am. Soc. Mass Spectrom.* 10:1188–1211.
31. Thalassinos, K., M. Grabenauer, …, J. H. Scrivens. 2009. Characterization of phosphorylated peptides using traveling wave-based and drift cell ion mobility mass spectrometry. *Anal. Chem.* 81:248–254.
32. Wiltzius, J. J., S. A. Sievers, …, D. Eisenberg. 2008. Atomic structure of the cross-beta spine of islet amyloid polypeptide (amylin). *Protein Sci.* 17:1467–1474.
33. Luca, S., W. M. Yau, …, R. Tycko. 2007. Peptide conformation and supramolecular organization in amylin fibrils: constraints from solid-state NMR. *Biochemistry.* 46:13505–13522.
34. Ridgway, Z., X. Zhang, …, D. P. Raleigh. 2018. Analysis of the role of the conserved disulfide in amyloid formation by human islet amyloid polypeptide in homogeneous and heterogeneous environments. *Biochemistry.* 57:3065–3074.
35. Thompson, M. J., S. A. Sievers, …, D. Eisenberg. 2006. The 3D profile method for identifying fibril-forming segments of proteins. *Proc. Natl. Acad. Sci. USA.* 103:4074–4078.
36. Chakraborty, S., B. Chatterjee, and S. Basu. 2012. A mechanistic insight into the amyloidogenic structure of hIAPP peptide revealed from sequence analysis and molecular dynamics simulation. *Biophys. Chem.* 168–169:1–9.
37. Tartaglia, G. G., and M. Vendruscolo. 2008. The Zyggregator method for predicting protein aggregation propensities. *Chem. Soc. Rev.* 37:1395–1401.
38. Garbuzynskiy, S. O., M. Y. Lobanov, and O. V. Galzitskaya. 2010. FoldAmyloid: a method of prediction of amyloidogenic regions from protein sequence. *Bioinformatics.* 26:326–332.
39. Fernandez-Escamilla, A. M., F. Rousseau, …, L. Serrano. 2004. Prediction of sequence-dependent and mutational effects on the aggregation of peptides and proteins. *Nat. Biotechnol.* 22:1302–1306.
40. Hobbs, J. R., and A. D. Morgan. 1963. Fluorescence microscopy with thioflavine-T in the diagnosis of amyloid. *J. Pathol. Bacteriol.* 86:437–442.
41. LeVine, H., III 1993. Thioflavine T interaction with synthetic Alzheimer's disease beta-amyloid peptides: detection of amyloid aggregation in solution. *Protein Sci.* 2:404–410.
42. Sulatskaya, A. I., A. A. Maskevich, …, K. K. Turoverov. 2010. Fluorescence quantum yield of thioflavin T in rigid isotropic solution and incorporated into the amyloid fibrils. *PLoS One.* 5:e15385.
43. Cloe, A. L., J. P. Orgel, …, S. C. Meredith. 2011. The Japanese mutant Aβ (ΔE22-Aβ(1-39)) forms fibrils instantaneously, with low-thioflavin T fluorescence: seeding of wild-type Aβ(1-40) into atypical fibrils by ΔE22-Aβ(1-39). *Biochemistry.* 50:2026–2039.
44. Young, L. M., P. Cao, …, S. E. Radford. 2014. Ion mobility spectrometry-mass spectrometry defines the oligomeric intermediates in amylin amyloid formation and the mode of action of inhibitors. *J. Am. Chem. Soc.* 136:660–670.
45. Bram, Y., A. Frydman-Marom, …, E. Gazit. 2014. Apoptosis induced by islet amyloid polypeptide soluble oligomers is neutralized by diabetes-associated specific antibodies. *Sci. Rep.* 4:4267.
46. Weise, K., D. Radovan, …, R. Winter. 2010. Interaction of hIAPP with model raft membranes and pancreatic beta-cells: cytotoxicity of hIAPP oligomers. *ChemBioChem.* 11:1280–1290.
47. Chen, M. S., D. S. Zhao, …, Y. M. Li. 2013. Characterizing the assembly behaviors of human amylin: a perspective derived from C-terminal variants. *Chem. Commun. (Camb.).* 49:1799–1801.
48. Bitan, G., and D. B. Teplow. 2004. Rapid photochemical cross-linking—a new tool for studies of metastable, amyloidogenic protein assemblies. *Acc. Chem. Res.* 37:357–364.
49. Abedini, A., A. Plesner, …, A. M. Schmidt. 2016. Time-resolved studies define the nature of toxic IAPP intermediates, providing insight for anti-amyloidosis therapeutics. *eLife.* 5:e12977.
50. Koo, B. W., and A. D. Miranker. 2005. Contribution of the intrinsic disulfide to the assembly mechanism of islet amyloid. *Protein Sci.* 14:231–239.
51. Marek, P. J., V. Patsalo, …, D. P. Raleigh. 2012. Ionic strength effects on amyloid formation by amylin are a complicated interplay among Debye screening, ion selectivity, and Hofmeister effects. *Biochemistry.* 51:8478–8490.
52. Wong, A. G., C. Wu, …, D. P. Raleigh. 2016. Analysis of the amyloidogenic potential of pufferfish (*Takifugu rubripes*) islet amyloid polypeptide highlights the limitations of thioflavin-T assays and the difficulties in defining amyloidogenicity. *Biochemistry.* 55:510–518.
53. Lee, K. H., A. Zhyvoloup, and D. Raleigh. 2019. Amyloidogenicity and cytotoxicity of Des-Lys-1 human amylin provides insight into amylin self-assembly and highlights the difficulties of defining amyloidogenicity. *Protein Eng. Des. Sel.* 32:87–93.
54. Fooks, H. M., A. C. Martin, …, E. G. Hutchinson. 2006. Amino acid pairing preferences in parallel beta-sheets in proteins. *J. Mol. Biol.* 356:32–44.
55. Zhang, N., J. Ruan, …, T. Zhang. 2009. The interstrand amino acid pairs play a significant role in determining the parallel or antiparallel orientation of beta-strands. *Biochem. Biophys. Res. Commun.* 386:537–543.
56. Wasmer, C., A. Lange, …, B. H. Meier. 2008. Amyloid fibrils of the HET-s(218-289) prion form a beta solenoid with a triangular hydrophobic core. *Science.* 319:1523–1526.